THE JOURNAL OF PHYSICAL CHEMISTRY C
A JOURNAL OF THE AMERICAN CHEMICAL SOCIETY

pubs.acs.org/JPCC

Article

# Hexagonal Boron Nitride Modulates Crystallinity and Charge Mobility in Poly(ethylene oxide)−$NaNO_3$ Electrolytes

Shreyas Pathreeker, Colby A. Snyder, George V. Papamokos, and Russell J. Composto*

Cite This: *J. Phys. Chem. C* 2024, 128, 38−49

Read Online

ACCESS | Metrics & More | Article Recommendations | Supporting Information

**ABSTRACT:** Composite solid polymer electrolytes (CSPEs) for solid-state sodium (Na) batteries are attractive due to their high modulus, good mechanical properties, and overall safety relative to liquid electrolytes. Important CSPE properties, such as crystallinity and ionic conductivity, are closely tied to the physicochemical characteristics of the filler material. In this work, we investigate how 2D hexagonal boron nitride (2D h-BN) flakes influence polymer crystallinity and ionic conductivity in poly(ethylene oxide) (PEO)-based CSPEs for Na-ion conduction using $NaNO_3$ as a model salt. Using X-ray diffraction (XRD), differential scanning calorimetry (DSC), and electrochemical impedance spectroscopy (EIS), we find that polymer crystallinity increases in the presence of the h-BN flakes, whereas the total ionic conductivity decreases relative to h-BN-free samples. Quantum mechanical DFT calculations reveal the ability of h-BN to bind with both ions of the dissociated salt, more strongly so with the $Na^+$ cation, which has hitherto not been reported in the context of Na-based polymer electrolytes. The combined experimental and computational efforts in this work provide key physical insights into the importance of filler geometry and chemical characteristics (i.e., Lewis acidity and Lewis basicity) in the design of CSPEs for Na-ion conduction.

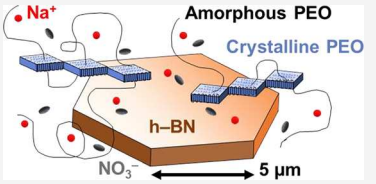




## 1. INTRODUCTION

Rapid electrification of vehicles and the increasing demand for stationary grid-level energy storage across the globe call into question the sustainability of Li-ion batteries (LIBs). Sodium (Na)-based batteries (both Na-ion and Na metal) have emerged as recognized alternatives to LIBs due to the relative abundance of Na, concerns with lithium supply, and the cost advantages that can be realized by optimizing Na batteries (such as by using aluminum as the current collector instead of copper).[1] The advantages of Na batteries are accompanied by drawbacks such as dendrite formation (when using Na metal as the anode) and lower energy density due to the higher standard reduction potential of Na than Li. Dendrite formation is a key safety issue and can be addressed using polymer electrolytes instead of liquid electrolytes. Polymer electrolytes can be categorized into composite solid polymer electrolytes (CSPEs) (i.e., polymer electrolytes containing a filler material dispersed in the polymer matrix), gel polymer electrolytes (GPEs), and neat solid polymer electrolytes (SPEs). A comprehensive review of progress in this area is available in the literature.[2,3]

The coupled nature of ion transport with polymer segmental motion in dual ion conductors, wherein both dissociated ions within the polymer matrix are mobile, has led to extensive efforts in polymer engineering to improve the ion transport and the overall electrochemical performance of the polymer electrolytes. Poly(ethylene oxide) (PEO) remains a popular choice for the polymer matrix in CSPEs due to its high dielectric constant and consequent ability to dissociate salts and form polymer−salt complexes as discovered over four decades ago.[4−6] Due to its extensive use in the literature, PEO is suitable for fundamental investigations of how filler particles affect ion transport. Based on the classical free-volume theory,[7,8] ion transport in semicrystalline polymer electrolytes occurs primarily in the amorphous domains of the polymer above its glass transition temperature $T_g$.

Various approaches, such as the plasticization of the polymer using a solvent[9,10] and the addition of filler particles to disrupt polymer crystallinity,[11,12] among others, have been attempted to improve the ionic conductivity of PEO-based polymer electrolytes for applications in LIBs and Na batteries. To this end, CSPEs containing filler materials such as particles, flakes, and rods are an exciting subclass of materials due to the synergistic effects of the filler material on the polymer matrix and ion transport properties. These effects include important factors such as changes in the glass transition temperature ($T_g$) of the polymer and ion dissociation, which impact ion transport properties. Importantly, the role of filler materials in CSPEs depends intricately upon the nature of filler−polymer interactions, filler size, and filler geometry.

Hexagonal boron nitride (h-BN) is an interesting filler due to its unique atomic structure, wherein boron is electrophilic and nitrogen is nucleophilic. Boron can therefore act as a Lewis acidic site and nitrogen as a Lewis basic site, thereby

Received: September 27, 2023
Revised: November 22, 2023
Accepted: December 13, 2023
Published: December 30, 2023

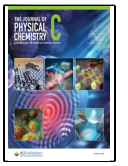

interacting with the dissociated salt in the polymer matrix. These interactions have been leveraged in several Li-based ion conductors to obtain improved cationic transference numbers,[13−17] which is a governing factor in electrolyte concentration polarization and battery performance.[18] In addition to its interaction with dissociated salt, h-BN can also mechanically reinforce the polymer[19,20] and improve its thermal properties[21,22] which can improve CSPE performance. Furthermore, 2D h-BN can induce interesting changes in CSPEs due to its flake-like morphology, which can in-turn affect PEO crystallization and structure. For instance, Tong et al.[23] added 2D graphene sheets to PEO and observed an increase in the number of nucleation sites during PEO crystallization. Similar findings have been reported by Sajid and co-workers[24] in an h-BN−PEO composite for humidity sensing applications, and by Biccai et al.[25] in $MoS_2$−PEO composites for piezoresistive applications. Introduction of polymer crystallinity due to BN addition has also been observed in a polyaniline (PANI)−BN polymer composite system.[26] In the context of polymer electrolytes, changes in polymer $T_g$ due to filler addition have been reported in early work on CSPEs.[27−29] Therefore, given the unique structural and chemical characteristics of h-BN and the semicrystalline nature of PEO, a combination of these materials presents an interesting physical system.

In the context of energy storage, investigations of structure−property relationships in BN-containing polymer electrolytes for Na-ion conduction are lacking. To the best of our knowledge, only a handful of recent reports have devoted attention to such polymer electrolyte systems.[30−34] Only one of these reports is based on a CSPE for Na-ion conduction, whereas the remainder of the studies is based on the incorporation of boron into the polymer chain rather than adding a BN-based filler to the polymer matrix. Chen et al.[30,31] chemically incorporated boron into polymer chains and found a decrease in the total ionic conductivity compared to full-carbon polymer matrices. However, increased cation transference was observed due to the anion-trapping ability of boron. Similar findings along with increased ionic conductivity have been reported by Genier and co-workers.[32] Last, the physical incorporation of boron nitride nanosheets to GPEs by Liu and co-workers resulted in a marginal increase in total ionic conductivity.[33,34] While salts with low lattice energies and anions with high delocalization of charge are preferred for ionic conductivity enhancement, we choose $NaNO_3$ as a model salt in this work owing to its low cost and ease of availability, with the focus being on the effect of filler addition on structure−property relationships in the CSPEs. Notably, $NaNO_3$ has received little attention, with only two reports on its use in ether-based electrolytes such as PEO.[35,36]

Given the nascency of incorporating h-BN into Na polymer electrolytes and the unique properties of h-BN, we explore here the PEO/sodium nitrate ($NaNO_3$)/h-BN system with particular emphasis on the influence of h-BN on polymer crystallinity and ionic conductivity. The effect of filler materials on the ionic conductivity in PEO−$NaNO_3$ complexes has not been investigated to date, which is the focus of the current work. Furthermore, we employ non-isothermal cooling to mimic the crystallization conditions encountered in roll-to-roll or other real-world processing conditions. Using X−ray diffraction (XRD) and differential scanning calorimetry (DSC), we find that h-BN has a nonmonotonic effect on polymer crystallinity and consequently ion transport properties of the CSPEs due to its flake-like morphology and binding (association) characteristics. Insights from density functional theory (DFT) calculations reveal the propensity for both dissociated ions to bind with h-BN, which we use to support our experimental findings. Our results suggest that filler geometry strongly influences the polymer structure, which in turn plays a governing role in CSPE electrochemical properties.

## 2. MATERIALS AND METHODS

**2.1. Materials.** Poly(ethylene oxide) (PEO, MW 35 kDa) and 99% sodium nitrate ($NaNO_3$) salt were purchased from Sigma Aldrich, Inc. The salt was vacuum-dried at 120 °C and 0.1" Hg vacuum for 16 h before use. Hexagonal boron nitride flakes (h-BN, approximately 5 $\mu$m wide × 80 nm thick) were purchased from US Research Nanomaterials and used as received.

**2.2. Sample Preparation.** Polymer electrolyte solutions were prepared by mixing PEO (repeat unit molar mass of 44.05 g/mol), $NaNO_3$ (molar mass of 85.00 g/mol), and h-BN flakes together in deionized water. Water was chosen as the solvent due to the limited solubility of $NaNO_3$ in acetonitrile, tetrahydrofuran, and methanol. The weight ratio of PEO to water for all samples was kept at 0.67:1. Appropriate amounts of salt were dissolved in the PEO−water−h-BN mixtures to obtain polymer electrolyte solutions containing EO:$Na^+$ in molar ratios of 24:1 and 4:1 representing a moderately concentrated and highly concentrated system, respectively. Here, EO refers to the etheric oxygen of the PEO chain. For each salt concentration, two h-BN weight loadings were explored: 0.3 wt % h-BN and 3 wt % h-BN with respect to the weight of PEO in the solutions. All three components were dissolved in glass vials, heated to 50 °C, and stirred for 1 h under ambient conditions. After the dissolution of $NaNO_3$, the vials were sonicated to disperse the h-BN flakes uniformly. CCSPE (with h-BN), and SPE (without h-BN) films were prepared by casting the solutions on glass slides and then evaporating the solvent. Representatively, 150 $\mu$L of the polymer electrolyte solution was pipetted and spread onto a clean glass slide approximately 6.45 $cm^2$ in area. The resulting films prior to drying were approximately 200 $\mu$m thick. The glass slide was placed on a hot plate at 120 °C for 1 h to evaporate the solvent before being transferred to a vacuum oven, where the samples were thoroughly dried under vacuum at 120 °C for 16 h. Once dry, the slides were transferred to a room temperature (22 °C) vacuum chamber and cooled for 1 h at a cooling rate of ca. 5 °C/min.

**2.3. Structural Characterization.** Optical microscopy in transmission mode was used to examine the dispersion of the h-BN nanoflakes within the CSPE and SPE films. X-ray diffraction (XRD) on the CSPE and SPE films was carried out using a Rigaku MiniFlex diffractometer with Cu K$\alpha$ radiation. Molecular interactions in the solid polymer electrolyte films were investigated using Fourier transform infrared spectroscopy (FTIR) carried out on a JASCO X6 spectrometer in attenuated total reflectance (ATR) mode using a resolution of 4 $cm^{-1}$. Differential scanning calorimetry (DSC) was carried out using a TA Instruments Q200 instrument at a heating rate of 10 °C/min.

**2.4. Electrochemical Impedance Spectroscopy.** Electrochemical impedance spectroscopy on the CSPE and SPE films was carried out using a Solartron ModuLab XM instrument in a frequency range of 1 MHz to 0.1 Hz under an applied AC voltage of 10 mV. In a typical measurement, a


https://doi.org/10.1021/acs.jpcc.3c06455
J. Phys. Chem. C 2024, 128, 38−49

rectangular piece of the CSPE and SPE film was cut using a clean razor blade, its dimensions (L × W × H) measured with a micrometer, and sandwiched between polished stainless-steel discs. Spectra were collected under vacuum in a temperature range of 298 to 328 K in 10 K intervals with a 20 min equilibration period at each temperature before collecting the spectrum. The ionic conductivity was determined using the equation:

$$\sigma = \frac{H}{Z \times A}$$

where $H$ is the thickness of the polymer electrolytes, $A$ is their surface area, and $Z$ is the real impedance extracted from the Bode plots.

**2.5. Density Functional Theory (DFT) Calculations.** Quantum-mechanical (QM) calculations were applied to calculate the complexation energy of the [h-BN/$Na^+$], [h-BN/$NO_3^-$], dimethoxyethane (DME)/$Na^+$, and $DME_2$/$Na^+$ pairs (DME is representative of the etheric oxygen of PEO). A $B_{12}N_{12}H_{12}$ molecule, following the formula $B_{3n}{}^2N_{3n}{}^2H_{6n}$ ($n$ = 2) adopted by Wu et al.,[37] was used to simulate the h-BN surface. The basis set superposition error (BSSE) was corrected by applying the counterpoise method.[38] The DFT-$\omega$B97X-D/aug-cc-pVDZ[39,40] level of theory and basis set were employed. Gaussian16 was used for all of the calculations reported in this work. The optimized structures are given in Cartesian coordinates in the Supporting Information

## 3. RESULTS AND DISCUSSION

**3.1. Dispersion of h-BN Flakes in the Polymer Electrolytes.** Dispersion of the filler in a polymer matrix is critical to the physicochemical properties of the resulting polymer composites.[41−43] Therefore, we first investigated the dispersion of h-BN flakes within the polymer (electrolyte) matrix using optical microscopy, which is appropriate to capture the h-BN flakes dispersed in the polymer matrix due to the micrometer-sized flakes. The characteristic Maltese-cross-type spherulitic morphology of melt-crystallized PEO is visible in several samples, as shown in Figure 1. Spherulites are qualitative indicators of polymer crystallinity, and doping with salt can affect PEO crystallinity, which we investigate based on spherulite size from the optical microscope images. The largest spherulite(s) are observed for neat PEO (Figure 1a1), and doping with salt progressively reduces the spherulite size from ca. 1 mm to ca. 100 $\mu$m, indicating the suppression of PEO crystallinity (Figure 1a1,b1,c1). This reduction in spherulite size is due to the formation of polymer−salt complexes, which is discussed and confirmed in later sections.

For neat PEO (Figure 1a1−a3), adding h-BN leads to changes in spherulite from ca. 1 mm to between 300 and 500 $\mu$m, but no clear trend is evident as a function of h-BN loading. However, the reduced spherulite size upon both salt and h-BN addition relative to pure PEO indicates changes to polymer crystallinity, which will be quantified in later sections. More importantly, we characterize the dispersion of h-BN flakes within the polymer matrix based on the contrast difference between the polymer matrix and the h-BN flakes.

Dark spots represent individual h-BN flakes, whereas black spots represent thicker stacks of h-BN flakes. The lateral dimension of the flakes is between 2 and 8 $\mu$m (see insets), and the dispersion of the h-BN flakes within the polymer matrix appears to be uniform without any notable large aggregates. The black spots are collections of individual h-BN flakes

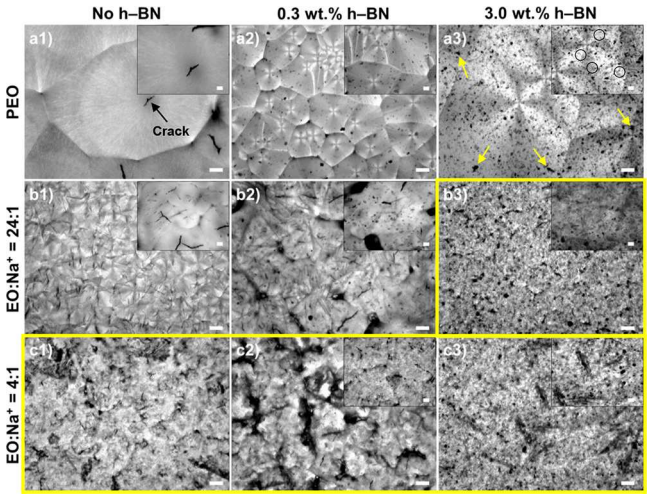


**Figure 1.** Top-down optical microscope images of the polymer electrolyte samples. Rows (top to bottom) present the pure PEO, $(PEO)_{24}$:$Na^+$, and $(PEO)_4$:$Na^+$. Columns (left to right) present the samples containing no h-BN flakes, 0.3 wt % h-BN flakes, and 3.0 wt % h-BN flakes. Scale bars in the main images are 100 $\mu$m, and those in the insets are 10 $\mu$m. The black arrow in (a1) points to the growth center of a spherulite, and the yellow arrows in (a3) point to the stacked flakes, whereas the black circles in the inset of (a3) present the collections of well-dispersed flakes. The yellow box indicates samples that exhibit fewer spherulites relative to the other samples, which suggests suppressed polymer crystallinity.

stacked on top of one another across the thickness (about 200 $\mu$m) of the polymer film. Overall, these microscope images indicate good dispersion of the h-BN flakes within the polymer (electrolyte) matrix, owing to which their effect on the electrolyte structure and ionic conductivity is expected to be uniform. We note that the h-BN loadings used in this work (0.3 and 3.0 wt %) correspond to a volume fraction of 0.16 and 1.62%, which are both less than the 1.88% critical volume for percolation (or percolation threshold) calculated using percolation theory.[44]

**3.2. PEO (Electrolyte) Crystallinity.** Polymer crystallinity is known to be altered by the addition of salt or filler material. Using XRD analysis, we investigate changes in the structure of the polymer (PEO) host due to the addition of h-BN flakes and $NaNO_3$, as shown in Figure 2. Polymer crystallinity is analyzed based on the two primary peaks at 19 and 23° exhibited by pure PEO. The peak at 19° is indexed to the [120] crystal plane, and that at 23° is attributed to the [032] crystal plane.[45−47] Changes in peak intensity, peak position, and peak width are direct manifestations of changes in PEO crystallinity caused by the PEO−salt interaction and/or PEO−h-BN interactions.

Peak shifts in XRD represent changes in unit cell dimensions of the polymer matrix, in this case the lamellar $d$-spacing of PEO. In the case of salt-free systems, no significant changes are detected to the two PEO peaks when h-BN is added to PEO, indicating little to no change in the underlying crystal structure of the PEO−h-BN composites. In the case of the salt-doped systems (i.e., the SPEs and CSPEs), the PEO peak positions shift to a lower $2\theta$ for both $(PEO)_{24}$:$Na^+$ and $(PEO)_4$:$Na^+$ samples, indicating a larger lamellar $d$-spacing of PEO upon the addition of salt to PEO. This shift indicates the formation of PEO−salt complexes, i.e., the insertion of $Na^+$ cations into the PEO lamellae. Similar downshifts in the characteristic PEO


https://doi.org/10.1021/acs.jpcc.3c06455
J. Phys. Chem. C 2024, 128, 38−49

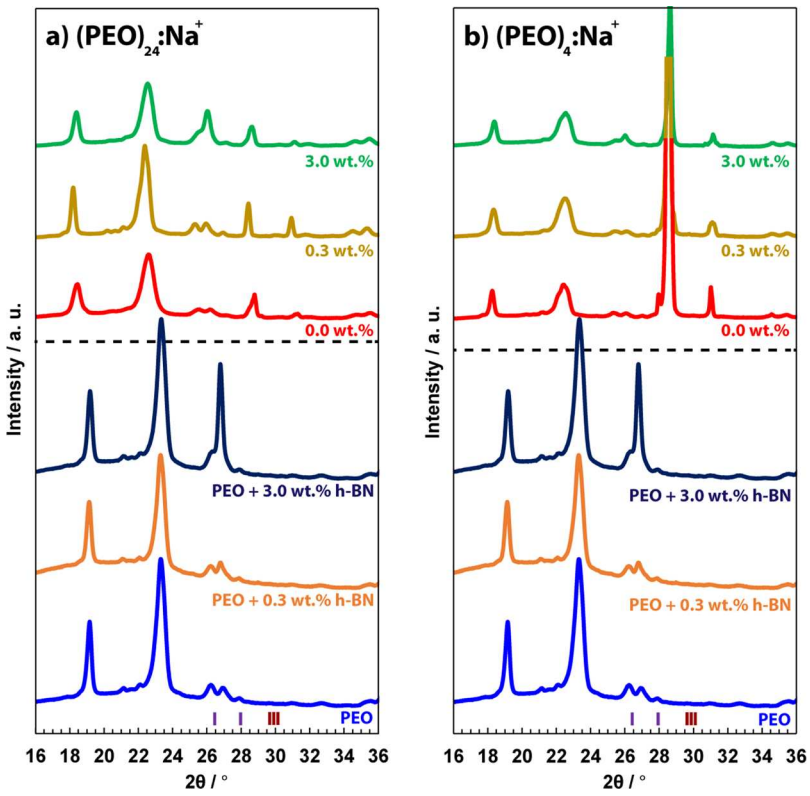


**Figure 2.** XRD patterns for (a) the $(PEO)_{24}$:$Na^+$ samples and (b) the $(PEO)_4$:$Na^+$ samples. Dashed horizontal lines separate the salt-free PEO samples from the salt-doped ones (i.e., bottom half shows pure PEO and top half shows polymer electrolytes). Colored bars at the bottom (L−R) represent the h-BN peaks (26.5° and 28°) and $NaNO_3$ peaks (triplet at ca. 30°), respectively.

peaks have been reported for both Na- and Li-based electrolytes.[35,48,49] A sharp crystalline peak indexed to crystalline $NaNO_3$ is observed at ca. 30° for all of the $(PEO)_4$:$Na^+$ samples, based on which we can conclude that these samples contain salt crystals. The initial liquid formulations prepared are optically transparent, and therefore, the salt crystals originate during cooling and crystallization owing to limited solubility in the polymer matrix. The salt peak appears at much lower intensities in the $(PEO)_{24}$:$Na^+$ samples, indicating better solubility of the salt in the polymer matrix at this salt concentration. Note that the salt peak in the polymer electrolytes appears at a lower $2\theta$ relative to bulk salt, which may be due to the presence of polymers within the salt crystals in the PEO−salt matrix.

Next, we use the PEO peak intensities and peak widths to investigate the polymer crystallinity in the salt-doped systems. The primary PEO peaks appear at lower intensities and are wider relative to those of pristine PEO. This peak broadening and reduction in peak intensities indicate that the addition of salt reduces PEO crystallinity, which is attributed to dative bond formation between the ether O atom of PEO and the $Na^+$ cation dissociated from the $NaNO_3$ salt. As such, it is a direct indicator of polymer−salt complex formation originating from the partial amorphization of crystalline PEO chains due to PEO−$Na^+$ interactions.

Adding h-BN to the salt-doped PEO has interesting effects on the PEO crystalline structure. For both $(PEO)_{24}$:$Na^+$ and $(PEO)_4$:$Na^+$ samples, adding 0.3 wt % h-BN leads to taller crystalline peaks relative to h-BN-free samples, indicating the increased polymer crystallinity relative to the sample without any h-BN. When the h-BN content is increased to 3.0 wt %, the peak intensities revert to nearly those of the sample without h-BN, indicating reduced polymer crystallinity. This nonmonotonic trend may be explained by the competition between nucleation and confinement-induced frustration of PEO polymer chains by the h-BN flakes. At the 0.3 wt % h-BN concentration, the number of h-BN flakes is insufficient to significantly disrupt PEO crystallinity. However, the h-BN flakes can promote PEO crystallization (via heterogeneous nucleation) due to their surface area, which reflects in the higher peak intensities. The surface area of the flakes should be proportionally larger at the 3.0 wt % h-BN concentration, resulting in an even higher polymer crystallinity, but since the number of flakes is also much larger than with 0.3 wt % h-BN, PEO spherulite growth is hindered and the overall polymer crystallinity decreases. This phenomenon manifests as shorter, broad peaks in the XRD data. Such behavior was reported previously in the literature. Li and co-workers described a similar phenomenon in their PEO/LiTFSI/$Ti_3C_2T_x$ composite polymer electrolyte system[50], wherein the $Ti_3C_2T_x$ filler possesses a 2D-flake morphology similar to the h-BN flakes used in our work. Interestingly, these authors found the nucleation effect to dominate at a filler loading of 0.38 wt % where PEO crystallinity increased, whereas beyond which the PEO crystallinity decreased. Similar findings have also been reported using multiwalled carbon nanotubes (MWCNTs)[51] as well as in PEO/$Ti_3C_2T_x$ composites (i.e., without salt).[52] Our observations are in close agreement with these and other reports[24,25] in the literature. Besides the weight percent of h-BN, the size of the flakes also plays a role in how h-BN impacts polymer crystallization. The lateral size of h-BN in this study is ∼5 $\mu$m, which is essentially a planar surface for nucleating PEO


https://doi.org/10.1021/acs.jpcc.3c06455
J. Phys. Chem. C 2024, 128, 38−49

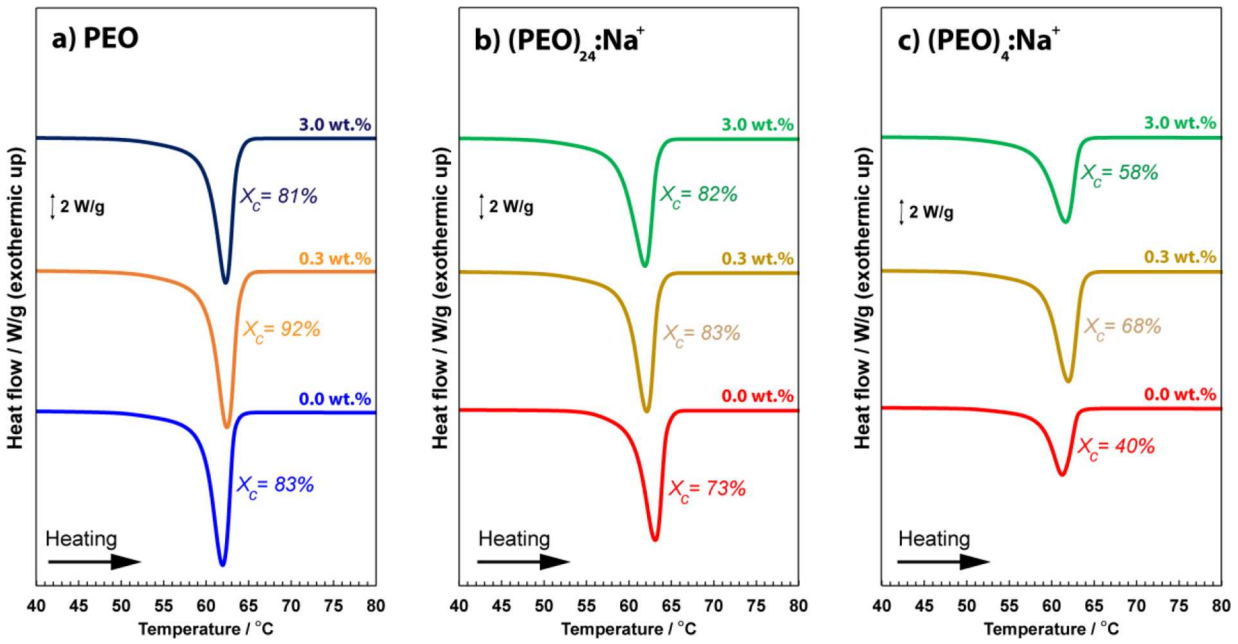


**Figure 3.** DSC heating traces for (a) PEO (no salt), (b) $(PEO)_{24}$:$Na^+$, and (c) $(PEO)_4$:$Na^+$. The inset text indicates the percent crystallinity ($X_c$) of the samples. Also indicated on the far right of each heating trace is the weight loading of h-BN flakes in the sample.

lamellae that can then form the large spherulites as seen in Figure 1.

We also used differential scanning calorimetry (DSC) to quantify the degree of crystallinity in the composite polymer electrolytes, as shown in Figure 3.

There is unambiguous evidence of increased PEO crystallinity upon the addition of 0.3 wt % h-BN to PEO with a decrease in the percent crystallinity upon increasing the loading of h-BN to 3.0 wt % (except for $(PEO)_{24}$:$Na^+$, 3.0 wt % h-BN where the percent crystallinity remains the same as the 0.3 wt % h-BN yet higher than the h-BN-free sample). Importantly, these trends closely match those seen in the XRD data (see Figure S1 in the Supporting Information), and therefore, collectively support the idea of a nucleation-dominated effect at 0.3 wt % h-BN loading and a confinement-dominated effect at 3.0 wt % h-BN loading. These competing effects also influence the ionic conductivity of the polymer electrolytes as will be discussed later. The melting points ($T_m$) of the polymer electrolytes do not change significantly upon addition of h-BN and/or salt. On the other hand, the glass transition temperatures ($T_g$) decrease by ca. 2 °C upon the addition of h-BN to the polymer electrolytes. Additionally, doping with salt increases polymer $T_g$, which is indicative of PEO−salt complex formation. These values are summarized in Table 1.

In this section, we have found based on XRD and DSC analysis that the addition of salt to the PEO matrix leads to a decrease in PEO crystallinity, which is attributed to PEO−salt interactions. As such, improved ionic conductivity can be expected from these salt-doped systems, which contain higher fractions of amorphous polymer. However, the addition of h-BN to neat PEO and salt-doped PEO (i.e., polymer electrolytes) results in a nonmonotonic variation in polymer crystallinity. The polymer crystallinity of the polymer electrolytes containing h-BN is higher than or nearly the same as that of samples containing no h-BN. This overall increase in crystallinity can be attributed to the 2D morphology of h-BN,

**Table 1. Summary of the Percent Crystallinity ($X_c$), Glass Transition Temperature ($T_g$), and Melting Point ($T_m$) from DSC Heating Scans**

| system | DSC $X_c$ (%) | $T_g$ (°C) | $T_m$ (°C) |
|---|---|---|---|
| PEO, no h-BN | 83 | −57.0 | 62.0 |
| PEO, 0.3 wt % h-BN | 92 | −54.0 | 63.0 |
| PEO, 3.0 wt % h-BN | 81 | −53.0 | 63.0 |
| $(PEO)_{24}$:$Na^+$, no h-BN | 73 | −53.5 | 63.5 |
| $(PEO)_{24}$:$Na^+$, 0.3 wt % h-BN | 83 | −56.0 | 62.0 |
| $(PEO)_{24}$:$Na^+$, 3.0 wt % h-BN | 82 | −55.0 | 62.0 |
| $(PEO)_4$:$Na^+$, no h-BN | 40 | −54.5 | 61.5 |
| $(PEO)_4$:$Na^+$, 0.3 wt % h-BN | 68 | −53.5 | 62.5 |
| $(PEO)_4$:$Na^+$, 3.0 wt % h-BN | 58 | −52.5 | 62.5 |

which adds surface area (and more nucleation sites) to the polymer matrix, thereby facilitating nucleation and crystallite growth wherein the flakes can serve as nucleation sites. Between the two h-BN loadings explored, we find that samples containing 0.3 wt % h-BN exhibit a higher polymer crystallinity than those containing 3.0 wt % h-BN. This effect is attributed to spherulitic disruption due to the closer interparticle spacing of the h-BN flakes at a higher weight loading of h-BN as also seen in the optical microscope images in Figure 1.

**3.3. Investigation of Polymer−Salt Complex Formation Using Vibrational Spectroscopy.** In this section, we further investigate the complexation in polymer electrolytes using FTIR. Figure 4 shows the FTIR spectra for the $CH_2$ rocking mode and combined asymmetric stretching mode of the C−O−C moiety of PEO and its associated changes upon the addition of $NaNO_3$ and different weight fractions of the h-BN flakes.

We first investigate the effect of adding salt and h-BN to the $CH_2$ moiety of PEO. Neat PEO demonstrates a nearly symmetric single peak centered at 840 $cm^{-1}$ due to the rocking mode of the $CH_2$ linkage. There are no appreciable changes in the $CH_2$ rocking mode upon addition of h-BN as evidenced by the nearly similar peak widths for the three samples: PEO,


https://doi.org/10.1021/acs.jpcc.3c06455
J. Phys. Chem. C 2024, 128, 38−49

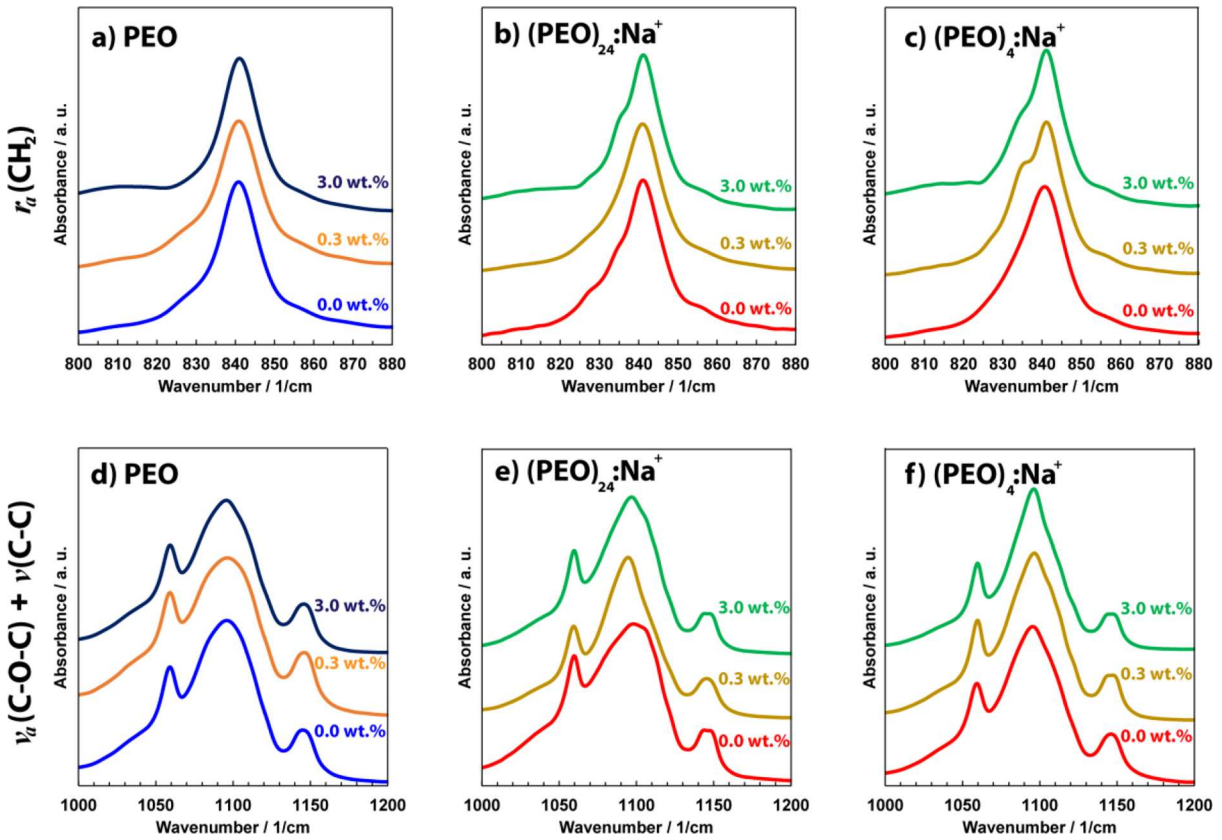


**Figure 4.** FTIR spectra for (L−R) neat PEO (no salt), $(PEO)_{24}$:$Na^+$, and $(PEO)_4$:$Na^+$. The top row shows the asymmetric rocking mode of $CH_2$, and the bottom row shows the combined vibrational modes of the C−O−C linkage and C−C bond of the PEO backbone.

PEO−0.3 wt % h-BN, and PEO−3.0 wt % h-BN. Upon adding salt, however, a shoulder peak develops in the $CH_2$ mode at ∼834 $cm^{-1}$ for both salt concentrations investigated. This peak may originate from either the PEO−salt complexation or crystalline $NaNO_3$, which exhibits an overlapping peak centered at the same wavenumber as the shoulder peak (see Figure S2a in the Supporting Information). To verify whether this peak belongs to a fraction of crystalline salt, we refer to the XRD data shown in Figure 1. Small crystalline salt peaks can be seen for $(PEO)_{24}$:$Na^+$, which suggests that the FTIR shoulder peak in the case of $(PEO)_{24}$:$Na^+$ (with and without h-BN) likely originates from salt crystals. We also note that the peak position for the primary $CH_2$ peak remains unchanged upon addition of either salt or h-BN, which suggests that the $CH_2$ mode itself does not partake in coordination or hydrogen bonding due to its locally nonpolar nature. For the $(PEO)_4$:$Na^+$ samples, the XRD data reveals a sharp crystalline peak from $NaNO_3$, indicating that the shoulder peak at 834 $cm^{-1}$ in the FTIR data also stems from crystalline salt. However, it is clear that the shoulder peaks are more prominent for $(PEO)_4$:$Na^+$ than $(PEO)_{24}$:$Na^+$, which may be attributed to the larger crystalline salt fraction in the former relative to the latter. Ionic conductivity is directly proportional to the number density of charge carriers in the conducting medium, and the strong presence of crystalline salt for $(PEO)_4$:$Na^+$ samples may counter the effect of the increased dissociated charge carriers. Therefore, one may posit that although the overall number of charge carriers with $(PEO)_4$:$Na^+$ is higher than that for $(PEO)_{24}$:$Na^+$, the presence of crystalline salt in the former could hinder ion transport and consequently lower the ionic conductivity in the CSPEs due to a lower effective free ion concentration. Typically, the anion peak in a polymer electrolyte containing a dissociated salt can be tracked to provide direct insights into its pairing characteristics by quantifying the FTIR data. In this work, however, the nitrate ion peak is degenerate with a PEO peak and therefore could not be used for analysis (see Figure S2b in the Supporting Information).

Next, we focus on the PEO C−O−C rocking mode vibrations shown in Figure 4. The C−O−C mode is appropriate for investigating polymer salt complexation because it captures the primary coordinating moiety of the polymer backbone, which is the ether O atom. All spectra indicate the classic triplet signature for semicrystalline PEO (1055, 1100, and 1145 $cm^{-1}$),[53,54] indicating that neat PEO, the PEO−salt complex, and PEO−salt−h-BN complexes are all semicrystalline for both salt compositions explored. These peaks represent the C−O−C segment in both the crystalline and the amorphous domains of PEO and as such evolve with complexation with salt. Subtle but noticeable changes in the shape of the main peak at 1100 $cm^{-1}$ are observable in the spectra, which we will use to analyze intercomponent interactions within the polymer electrolyte.

Addition of salt leads to peak broadening, which confirms polymer−salt complex formation.[53,54] More specifically, we expect this complex formation to originate from interactions between the ether of PEO and the $Na^+$ ion of the salt following its dissociation. The peak narrows when 0.3 wt % h-BN is added, and a similar narrowing of the peak is also observed at the higher h-BN weight fraction of 3.0 wt %. Importantly, we employ density functional theory (DFT) calculations to better understand the intercomponent interactions in our polymer


https://doi.org/10.1021/acs.jpcc.3c06455
J. Phys. Chem. C 2024, 128, 38−49

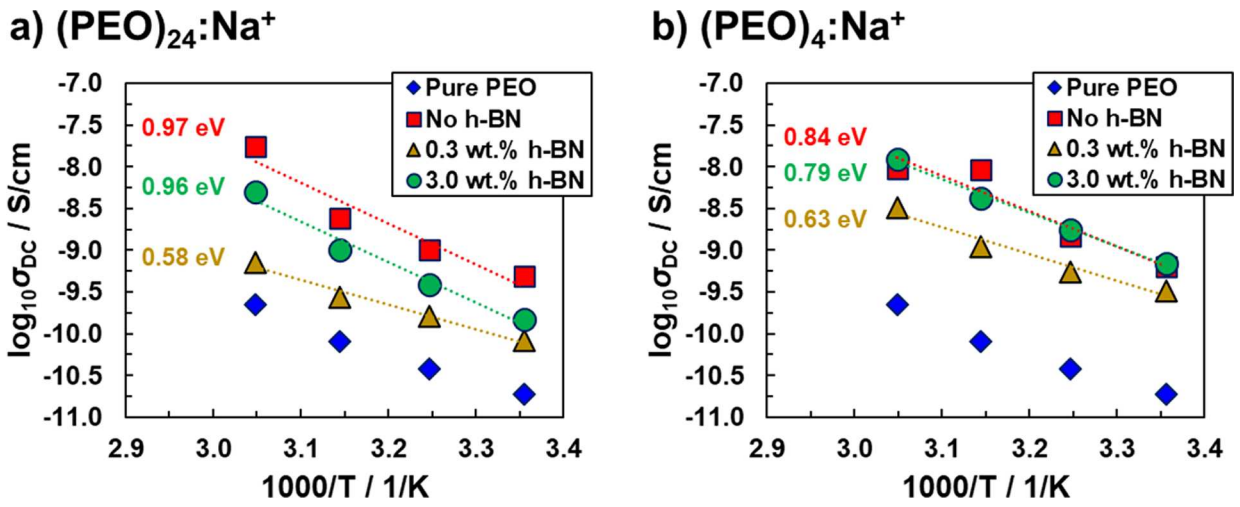


**Figure 5.** Arrhenius plots of total ionic conductivity for (a) $(PEO)_{24}$:$Na^+$ samples and (b) $(PEO)_4$:$Na^+$ samples in a temperature range of 25 to 55 °C in steps of 10 °C. Dashed lines are linear fits to the data, and inlaid text indicates the activation energies obtained from the natural logarithms of ionic conductivity as a function of inverse temperature.

electrolytes (shown later), which support the changes seen in the FTIR spectra. Narrowing of the C−O−C peak upon the addition of h-BN indicates a change in the solvation structure of the polymer electrolytes. Since the total number of charge carriers in the h-BN-free and h-BN-containing samples is the same for any given salt concentration, the change in PEO−salt complexation upon h-BN addition must originate from interactions between h-BN and $NaNO_3$ and from changes to the PEO crystalline structure induced by the addition of h-BN. Reduced polymer-salt complexation upon h-BN addition implies that the dissociated cations that were previously coordinated with PEO must now coordinate with another electroactive moiety in the electrolyte and/or recombine with the anion to form precipitates. The XRD data present evidence of salt precipitates in the polymer electrolytes, which is particularly evident for the $(PEO)_4$:$Na^+$ samples. However, $Na^+$ may coordinate with the N atom in h-BN as well as with the O atom in PEO, and the $NO_3^-$ anion can interact with the electrophilic B atom in h-BN. We investigated this possibility using FTIR analysis on $NaNO_3$−water−h-BN solutions but could not detect changes in the nitrate ion peak from h-BN addition, likely due to the low concentration of h-BN in the solutions (see Figure S3 in the Supporting Information).

Changes in the PEO backbone conformation were also investigated using FTIR analysis. This investigation is important because changes in PEO conformation can influence its ability to coordinate with metal cations. This point is highlighted by efforts on tuning the conformation of PEO to tune $Li^+$ ion conductivity.[55,56] Briefly, PEO in its *trans* (planar zigzag) configuration is less effective at coordinating with metal cations relative to its *gauche*/*helical* conformation, which can form an "envelope" and solvate metal cations. The reader is directed to the detailed structural models discussed by Ratner and co-workers.[57,58] Pure PEO takes the (CC−OC) *trans*-(CO−CC) *trans*-(CC−CO) *gauche*/*helical* [*TTG*] conformation at room temperature. Due to the ability of $CH_2$ modes to reflect polymer chain conformational changes, the O-$(CH_2)_2$-O linkage can be used to probe changes in the PEO backbone. Previous studies on the PEO-based electrolytes have established that vibrational bands between 800 and 950 $cm^{-1}$ are a signature of *gauche* (CC−CO) and *gauche* $CH_2$ modes.[36,57,58] Anantha and co-workers[36] reported identical peaks between pure PEO and PEO−$NaNO_3$ complexes in the 800 and 950 $cm^{-1}$ wavenumber range and concluded that the *gauche* conformation of PEO remains largely unchanged with salt complexation. However, careful inspection of our FTIR spectra in the 900 to 1000 $cm^{-1}$ wavenumber (see Figure S4a,b in the Supporting Information) range suggests otherwise. We observe that the peak at 962 $cm^{-1}$ in pure PEO evolves with addition of salt and the subsequent addition of h-BN. Indeed, this peak at 962 $cm^{-1}$ belongs to the *trans* conformation of PEO.[59,60] We quantified our FTIR data to extract information regarding the relative content of *trans* PEO conformers (962 $cm^{-1}$) to *gauche* PEO conformers (at 948 $cm^{-1}$) and correlated this ratio with the fwhm of the C−O−C peak(s) (see Figure S4c,d in the Supporting Information). Note that due to the interconnected nature of polymer crystallinity, polymer chain conformation, and complexation, we limit the conformational analysis to samples with and without h-BN. h-BN-doped samples exhibit a higher *trans* conformer content and a lower fwhm (i.e., polymer−salt complexation) than their h-BN-free counterparts. We note that this observation correlates with the polymer crystallinity from our XRD and DSC analysis.

Overall, FTIR analysis confirms the formation of PEO−salt complexes, with the addition of h-BN altering the solvation structure of the complexes. The decrease in polymer crystallinity upon salt incorporation results from $NaNO_3$ dissociation in the polymer matrix and consequent polymer−cation interactions. This makes $Na^+$ and $NO_3^-$ the charge carriers in the SPEs and CSPEs. Due to stringent drying conditions, we expect the contribution of proton conduction to be negligible. These findings in conjunction with the discussion on polymer electrolyte structure are expected to influence the electrochemical properties of the polymer electrolytes, which is discussed in the next section.

**3.4. Ionic Conductivity and Binding Energy.** In this section, we correlate structural changes in the polymer electrolytes with their ion transport properties using electrochemical impedance spectroscopy (EIS), as shown in Figure 5. Total ionic conductivities ($\sigma$) were calculated using impedances obtained from Bode plots (see Figure S5 in the Supporting Information).

We investigated the total ionic conductivity of the SPEs and CSPEs as a function of temperature. First, pure PEO


https://doi.org/10.1021/acs.jpcc.3c06455
J. Phys. Chem. C 2024, 128, 38−49

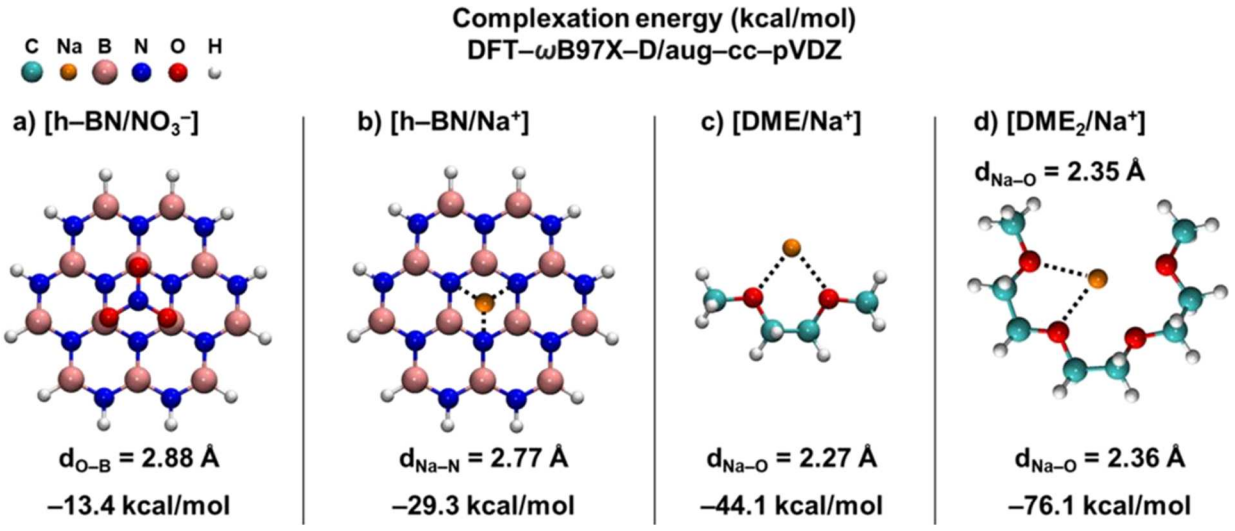


**Figure 6.** Optimized geometries and corresponding DFT binding energies for (a) the [h-BN/$NO_3^-$] pair, (b) the [h-BN/$Na^+$] pair, (c) the [EO/$Na^+$] complex, and (d) the [$(EO)_2/Na^+$] complex. Legend of the colors is indicated at the top left.

demonstrates a room temperature ionic conductivity on the order of $10^{-11}$ S/cm, which is likely due to impurities in the polymer and not from ionic charge carriers. Note that the ionic conductivity for pure PEO is about 2 orders of magnitude lower than that of the salt-doped PEO. We attribute this relatively small difference to the low dissociation of the salt. Although $NaNO_3$ was chosen as a model salt, salts such as NaFSI are much better at dissociation and consequently at improving the ionic conductivity, as described in future studies. $\sigma$ for the $(PEO)_4$:$Na^+$ samples is higher than that for the $(PEO)_{24}$:$Na^+$ samples in accordance with the relationship between ionic conductivity and charge carrier concentration, i.e., a higher salt concentration must exhibit a higher ionic conductivity. For all samples investigated, the increase in $\sigma$ with increasing temperature indicates that the ionic conductivity mechanism is thermally activated, i.e., by hopping between coordinating sites on the polymer chain(s). We quantified the difference in $\sigma$ for the two salt concentrations using the ratio $\sigma_{4:1}/\sigma_{24:1}$ at room temperature. If based solely on the total charge carrier concentration and neglecting changes in polymer crystallinity, the $(PEO)_4$:$Na^+$ samples would be expected to be ca. 6 times more ionically conductive than their $(PEO)_{24}$:$Na^+$ counterparts. However, we find that the $(PEO)_4$:$Na^+$ samples are between 1.31 and 4.65 times more conductive than the $(PEO)_{24}$:$Na^+$ samples depending upon h-BN loading. Note that the XRD data in Figure 1 reveals a strong presence of salt crystals in the $(PEO)_4$:$Na^+$ samples and to a lesser extent in the $(PEO)_{24}$:$Na^+$ samples as well. Importantly in the case of the $(PEO)_4$:$Na^+$ samples, the true dissociated salt concentration would be lower than one $Na^+$ cation for four EO atoms, which could be the underlying reason behind the reduced ionic conductivity at higher salt concentrations.

For both salt concentrations explored, $\sigma$ follows the trend $\sigma_{\text{no h-BN}} > \sigma_{\text{3.0 wt \% h-BN}} > \sigma_{\text{0.3 wt \% h-BN}}$, and the crystalline PEO peak areas (PA) from XRD analysis follow the inverse trend as that of ionic conductivity, i.e., $PA_{\text{0.3 wt \% h-BN}} > PA_{\text{3.0 wt \% h-BN}} > PA_{\text{no h-BN}}$. Furthermore, correlation with our DSC results reveals that samples with the lowest percent crystallinity exhibit the highest $\sigma$ for any given salt concentration. This finding indicates that the competition between nucleation and confinement manifests as changes in the ionic conductivity of the polymer electrolytes, with the polymer crystallinity being modulated by the h-BN flakes. The total ionic conductivity observed in our work is nearly 2 orders of magnitude lower than that reported by others previously.[35,36] To reconcile this difference, we carried out a test experiment on an h-BN-free $(PEO)_4$:$Na^+$ sample to investigate the effect of moisture on $\sigma$. The drop-cast sample was dried at 120 °C for 1 h to remove solvent and then equilibrated under vacuum at room temperature with impedance spectra collected in situ. Our findings suggest that the ionic conductivity of the sample drops from $\sim 10^{-8}$ to $\sim 10^{-10}$ S/cm within 4 h of vacuum drying at ambient temperature (see Figure S6 in the Supporting Information). As such, our fully dried samples may demonstrate a lower ionic conductivity due to the absence of moisture (as also seen in the extended FTIR data shown in Figure S7 in the Supporting Information).

Ion complexation is central to ionic conductivity, and therefore, changes in ion complexation due to the addition of h-BN to the polymer electrolyte need to be considered. To this end, we carried out density functional theory (DFT) calculations to determine the binding energy between the different components in our polymer electrolytes. The results of the quantum mechanical (QM) calculations are presented in Figure 6. We investigated the binding energy for the following pairs: [EO/$Na^+$] representing polymer etheric oxygen−cation interactions, [h-BN/EO] representing h-BN−polymer etheric oxygen interactions, [h-BN/$Na^+$] representing h-BN−cation interactions, and [h-BN/$NO_3^-$] representing h-BN−anion interactions. We first tested various initial configurations of the [h-BN/$NO_3^-$] pair. As expected, the nitrate anion exhibits a strong repulsive force on the order of +35 kcal/mol (data not shown) when placed perpendicular to the h-BN plane with one oxygen atom facing a nitrogen atom. Placing the nitrate anion plane parallel to the h-BN plane results in an attractive force of −13.4 kcal/mol between the h-BN and nitrate anion when the oxygen atoms are above the boron atoms, as shown in Figure 6a. On the other hand, the $Na^+$ cation is attracted to h-BN with more than double the strength (−29.3 kcal/mol) with respect to the nitrate anion, as shown in Figure 6b. The symmetric arrangement of boron in h-BN prevents the stronger


https://doi.org/10.1021/acs.jpcc.3c06455
J. Phys. Chem. C 2024, 128, 38−49

interaction of the $Na^+$ cation with the nitrogen atoms of h-BN. This result suggests that the $Na^+$ cation binds more strongly to the h-BN than to the nitrate anion, i.e., h-BN is not only an anion trapper but also a stronger cation trapper, and this stems from the duality of its nature as both an electrophilic and nucleophilic material.

Next, we focused on the [EO/$Na^+$] binding characteristics. The complexation energy between a single DME unit and the $Na^+$ cation is −44.1 kcal/mol, while when two DME units are involved, this energy is −76.1 kcal/mol (Figure 6c,d). Consequently, the structure of the PEO chain and the number of oxygen atoms complexed with $Na^+$ determine the strength of the interaction. The PEO can elicit the $Na^+$ cation from h-BN by increasing the number of complexed oxygen atoms and its PEO monomeric units. These binding energies are within the same range as those found by others in the literature.[61,62] Note that the [h-BN/$Na^+$] binding energy is lower than the [EO/$Na^+$] binding energy, yet sufficiently strong to influence PEO−$Na^+$ complexation. This result is reflected in the FTIR spectra shown in Figure 2 wherein changes in the C−O−C peak width (and free charge carrier concentration) were observed upon h-BN addition. The distances of the ions from the h-BN atoms that generate the attraction are also shown in Figure 6. It is evident that shorter distances entail stronger interactions. For all cases, the distances of the ions from the h-BN and the monoglyme unit have a single value, revealing the symmetry of the interaction, except for the last case (Figure 6d), where the ethereal oxygen atoms are closer to the $Na^+$ cation by nearly 0.01 Å.

These findings have important implications for Na-ion conduction in CSPEs containing BN filler. The strong interaction of h-BN with both dissociated ions (and not solely the anion as is usually implied) is bound to play an important role in ionic conductivity and cationic transference due to changes in the charge carrier concentration. Specifically, the ability of both fully dissociated anions to interact favorably with h-BN is expected to lead to a decrease in the total ionic conductivity of the CSPEs, which is seen in our experimental EIS data. The increase in total ionic conductivity at 3.0 wt % h-BN loading may be attributed to the confinement-dominated effect on PEO crystallinity at that h-BN concentration, due to which PEO crystallinity decreases (from XRD and DSC data). This decrease in crystallinity is responsible for the slightly higher ionic conductivity observed at 3.0 wt % h-BN loading relative to the 0.3 wt % h-BN loading. The [h-BN/$Na^+$] binding energy is 2.2 times higher than the [h-BN/$NO_3^-$] binding energy. Thus, we can posit that the transference number is lower in the CSPEs containing h-BN compared to the PEO/$NaNO_3$ SPEs and overall less than 0.5. Recent systematic work investigating the relationship between PEO crystallinity and ionic conductivity in composite solid polymer electrolytes suggests that a 20% reduction in crystallinity can correspond to 1 order of magnitude increase in ionic conductivity.[63] Our experimental results for the 0.3 wt % h-BN and 3.0 wt % h-BN systems are indeed well within an order of magnitude of each other for both salt concentrations investigated. Last, our DFT results also indicate the affinity of PEO toward h-BN (see Figure S8 in the Supporting Information), which further supports the enhanced nucleation model. Yang et al.[33] reported a slightly higher ionic conductivity (×1.5) for BN nanosheet (BNNS)-containing Na gel polymer electrolytes relative to BN-free ones. The improvement in ionic conductivity was attributed to the anion-trapping ability of BNNS and the consequent increase in the free $Na^+$ concentration. Unlike the CSPEs in the present work wherein PEO is the only component capable of facilitating ion motion, the BNNS reported by Yang et al. have polyethylene glycol (PEG) chains grafted to their surface, which in turn improves ion transport. Furthermore, the GPEs used by these authors exhibit a high dielectric constant, low viscosity solvent, and as such, the solvation environment therein is vastly different than in solid-state polymer electrolytes. Wieczorek et al.[64] reported a similar nonmonotonic trend of ionic conductivity using Lewis acidic alumina particles in their CSPEs with $NaClO_4$ as the salt. Last, Li and co-workers[15] reported a lower ionic conductivity upon h-BN addition to solid PEO/LiTFSI electrolytes, which suggests that the role played by h-BN in CSPEs is system-dependent and cannot be readily generalized.

Next, we focus on the activation energy for ion transport in our polymer electrolytes. First, we find that the activation energies for the $(PEO)_4$:$Na^+$ samples are ca. 0.15 eV lower than those for the $(PEO)_{24}$:$Na^+$ samples (except for the 0.3 wt % h-BN samples, which are similar for both salt concentrations). The lower activation energy at higher salt concentrations is attributed to the higher number of free charge carriers. The activation energy for ion motion is ca. 0.60 eV for the 0.3 wt % h-BN samples and increases to 0.96 and 0.79 eV at 3.0 wt % h-BN for $(PEO)_{24}$:$Na^+$ and $(PEO)_4$:$Na^+$, respectively. Since the activation energy is associated with ion mobility, our observations indicate that ion mobility increases at 0.3 wt % h-BN loading and then decreases at 3.0 wt % h-BN loading. Ionic conductivity is a product of the magnitude of charge [$q$], the charge carrier concentration [$n$], and ion mobility [$\mu$], where [$\mu$] is associated with the activation energy required for transport.[65] [$q$] is taken to be constant for all samples herein, whereas the individual contributions of the remaining two factors to ionic conductivity can be discussed as follows. The lower ionic conductivity at 0.3 wt % h-BN may be due to a lower free charge carrier concentration, but the decrease in activation energy may be attributed to a decrease in $T_g$ of the polymer, which represents the segmental motion of the polymer (see Table 1). On the other hand, the increase in activation energy at 3.0 wt % h-BN may be attributed to the slightly increased polymer $T_g$ at that weight fraction of h-BN. Confinement of polymer chains in the presence of a larger number of h-BN flakes, tortuosity generated by the flakes, and salt crystals together can also increase the activation energy for ion hopping (i.e., hopping sites on the polymer chain(s) are less accessible). The overlapping FTIR spectra prevent the deconvolution of ions associated with h-BN, but the free charge carrier concentration may also demonstrate a non-monotonicity similar to that of the ionic conductivity and activation energy leading to such behavior.

Last, we propose two possible mechanisms by which the total ionic conductivity in our CSPEs is influenced by h-BN. Mechanism 1: changes in the C−O−C peak shape in the FTIR spectra upon h-BN addition indicate changes in the solvation structure of the $Na^+$ cations in the CSPEs. Given the strong binding of salt ions with h-BN, the h-BN flakes can partially scavenge dissociated salt ions from the PEO, thereby reducing the number of free charge carriers. Any dissociated ions coordinated with h-BN cannot contribute to the ionic conductivity due to the dependence of ion transport on polymer segmental motion and the inability of h-BN to aid in ion transport. As a result of this scavenging, the total ionic


https://doi.org/10.1021/acs.jpcc.3c06455
J. Phys. Chem. C 2024, 128, 38−49

conductivity of CSPEs decreases. PEO has a slightly higher dielectric constant than h-BN and therefore may more strongly bind with the metal cation than h-BN. As such, the changes in ionic conductivity are within an order of magnitude of each other for the two h-BN loadings explored. Furthermore, note that the total ionic conductivity is a summation of the ionic conductivity of fully dissociated cations and anions. Our DFT results show that preferential binding between the nitrate anion and h-BN is a distinct possibility. As such, the total ionic conductivity is naturally expected to decrease in the presence of h-BN, which our experimental data indicates. Mechanism 2: h-BN may improve the overall salt dissociation due to its binding characteristics, but the ionic conductivity is reduced by polymer crystallinity. Namely, nucleation enhances crystallinity, and the increase in charge carrier concentration may be countered by the reduction of amorphous polymer content in the CSPEs. On the other hand, confinement suppresses crystallinity, which together with the higher charge carrier concentration, may improve the ionic conductivity. However, we note that for $(PEO)_{24}$:$Na^+$, the total ionic conductivity at 3.0 wt % h-BN increases slightly relative to 0.3 wt % h-BN even though the reduction in crystallinity is small. This suggests that there may be factors in addition to bulk polymer crystallinity, such as altered polymer dynamics under interlayer confinement and adjacent to the surface(s) of the h-BN flakes, that can modulate ion transport in the CSPEs, which is the focus of ongoing work.

## 4. CONCLUSIONS

In this work, we find using XRD and DSC analysis that adding h-BN to the PEO−$NaNO_3$ polymer electrolytes has a nonmonotonic effect on polymer crystallinity. Additionally, FTIR confirms the PEO−$Na^+$ complex formation as well as changes to this complex upon h-BN addition. For both salt concentrations explored (EO/$Na^+$ = 24:1 and 4:1), surface-induced nucleation from the h-BN flakes dominates and polymer crystallinity increases at a low h-BN loading of 0.3 wt %, whereas increasing the h-BN weight loading 10-fold to 3.0 wt % leads to a decrease in polymer crystallinity due to the effect of polymer chain confinement by the h-BN flakes at spherulitic length-scales. The overall polymer crystallinity at any h-BN loading, however, is higher than that without h-BN, further indicating that the geometry of the filler plays an important role in CSPEs.

Using EIS, we find the highest ionic conductivity for samples containing no h-BN, indicating that h-BN effectively reduces the total ionic conductivity in this particular CSPE system. Intercomponent binding energies determined using DFT calculations suggest an affinity for both ions of the salt to interact favorably (i.e., attractive interactions) with the h-BN filler, which can lead to salt partitioning between the PEO and the h-BN flakes. The reduction in total ionic conductivity upon h-BN addition is within 1 order of magnitude of that for the h-BN-free samples. The h-BN flakes play a dual role in the CSPEs in this work, but their effect is nonmonotonic. At 0.3 wt % h-BN, the flakes appear to enhance polymer crystallinity while reducing the free charge carrier concentration by binding with dissociated ions, resulting in a lower ionic conductivity. At 3.0 wt % h-BN, the flakes suppress PEO spherulite growth and the ionic conductivity increases. Notably, under no case is the total ionic conductivity of h-BN-containing samples higher than the h-BN-free samples, which reinforces the dual-ion trapping ability of h-BN for Na-containing CSPEs.

This work has implications for the design and development of semicrystalline CSPEs containing 2D fillers with unique chemical characteristics for Na-ion conduction.

## ■ ASSOCIATED CONTENT

### Supporting Information

The Supporting Information is available free of charge at https://pubs.acs.org/doi/10.1021/acs.jpcc.3c06455.

Integrated peak areas from XRD data; additional FTIR data; conformational analysis; raw Bode plots of the polymer electrolytes; complex plot from EIS; [h-BN/EO] binding energy from DFT; and Cartesian coordinates of optimized pairwise geometries from DFT (PDF)

## ■ AUTHOR INFORMATION


### Corresponding Author

**Russell J. Composto** − *Department of Materials Science and Engineering and Department of Chemical and Biomolecular Engineering, University of Pennsylvania, Philadelphia, Pennsylvania 19104, United States;* orcid.org/0000-0002-5906-2594; Email: composto@seas.upenn.edu

### Authors

**Shreyas Pathreeker** − *Department of Materials Science and Engineering, University of Pennsylvania, Philadelphia, Pennsylvania 19104, United States;* orcid.org/0000-0001-7589-5345

**Colby A. Snyder** − *Department of Materials Science and Engineering, University of Pennsylvania, Philadelphia, Pennsylvania 19104, United States;* orcid.org/0009-0005-0956-7403

**George V. Papamokos** − *Department of Physics, Harvard University, Cambridge, Massachusetts 02138, United States;* orcid.org/0000-0002-7671-2798

Complete contact information is available at: https://pubs.acs.org/10.1021/acs.jpcc.3c06455


### Notes

The authors declare no competing financial interest.

## ■ ACKNOWLEDGMENTS

This research was supported by the National Science Foundation (NSF) under Future Manufacturing grant NSF-FMRG-2134715 (S.P., R.J.C.) with PI Prof. Eric Detsi, the Division of Materials Research Polymers Program under grant NSF-DMR-1905912 (R.J.C.), and the Vagelos Integrated Program in Energy Research (VIPER) undergraduate research program at the University of Pennsylvania (C.A.S.). The authors acknowledge use of the Dual Source and Environmental X-ray Scattering facility operated by the Laboratory for Research on the Structure of Matter at the University of Pennsylvania (NSF-MRSEC-DMR-2309043). Additionally, this work was carried out in part at the Singh Center for Nanotechnology at the University of Pennsylvania, which is supported by the NSF National Nanotechnology Coordinated Infrastructure Program under grant NSF-NNCI-2025608. The computational work in this paper was carried out on the FASRC Cannon cluster supported by the FAS Division of Science Research Computing Group at Harvard University, USA (G.V.P.). The authors thank Prof. Karen I. Winey for use of the potentiostat-frequency response analyzer in her lab, and

Dr. Chien-Hua Tu for useful discussions. The authors also thank Dr. Mahadevan Khantha for useful early discussions on DFT calculations.

## REFERENCES

(1) Usiskin, R.; Lu, Y.; Popovic, J.; Law, M.; Balaya, P.; Hu, Y. S.; Maier, J. Fundamentals, status and promise of sodium-based batteries. *Nature Reviews Materials* **2021**, *6* (11), 1020−1035.
(2) Yang, J.; Zhang, H.; Zhou, Q.; Qu, H.; Dong, T.; Zhang, M.; Tang, B.; Zhang, J.; Cui, G. Safety-enhanced polymer electrolytes for sodium batteries: recent progress and perspectives. *ACS Appl. Mater. Interfaces* **2019**, *11* (19), 17109−17127.
(3) Gebert, F.; Knott, J.; Gorkin, R., III; Chou, S. L.; Dou, S. X. Polymer electrolytes for sodium-ion batteries. *Energy Storage Materials* **2021**, *36*, 10−30.
(4) Wright, P. V. Electrical conductivity in ionic complexes of poly (ethylene oxide). *Br. Polym. J.* **1975**, *7* (5), 319−327.
(5) Payne, D. R.; Wright, P. V. Morphology and ionic conductivity of some lithium ion complexes with poly (ethylene oxide). *Polymer* **1982**, *23* (5), 690−693.
(6) Armand, M. Polymer solid electrolytes-an overview. *Solid State Ionics* **1983**, *9*, 745−754.
(7) Druger, S. D.; Ratner, M. A.; Nitzan, A. Polymeric solid electrolytes: Dynamic bond percolation and free volume models for diffusion. *Solid State Ionics* **1983**, *9*, 1115−1120.
(8) Ratner, M. A.; Johansson, P.; Shriver, D. F. Polymer electrolytes: ionic transport mechanisms and relaxation coupling. *MRS Bull.* **2000**, *25* (3), 31−37.
(9) Walker, C. W.; Salomon, M. Improvement of ionic conductivity in plasticized PEO-based solid polymer electrolytes. *J. Electrochem. Soc.* **1993**, *140* (12), 3409.
(10) Bandara, L. R. A. K.; Dissanayake, M. A. K. L.; Mellander, B. E. Ionic conductivity of plasticized (PEO)-$LiCF_3SO_3$ electrolytes. *Electrochim. Acta* **1998**, *43* (10−11), 1447−1451.
(11) Croce, F.; Appetecchi, G. B.; Persi, L.; Scrosati, B. Nanocomposite polymer electrolytes for lithium batteries. *Nature* **1998**, *394* (6692), 456−458.
(12) Croce, F.; Persi, L.; Scrosati, B.; Serraino-Fiory, F.; Plichta, E.; Hendrickson, M. A. Role of the ceramic fillers in enhancing the transport properties of composite polymer electrolytes. *Electrochim. Acta* **2001**, *46* (16), 2457−2461.
(13) Bian, X.; Liang, J.; Tang, X.; Li, R.; Kang, L.; Su, A.; Su, X.; Wei, Y. A boron nitride-polyvinylidene fluoride-co-hexafluoropropylene composite gel polymer electrolyte for lithium metal batteries. *J. Alloys Compd.* **2019**, *803*, 1075−1081.
(14) Zhang, Z.; Antonio, R. G.; Choy, K. L. Boron nitride enhanced polymer/salt hybrid electrolytes for all-solid-state lithium ion batteries. *J. Power Sources* **2019**, *435*, No. 226736.
(15) Li, Y.; Zhang, L.; Sun, Z.; Gao, G.; Lu, S.; Zhu, M.; Zhang, Y.; Jia, Z.; Xiao, C.; Bu, H.; Xi, K.; Ding, S. Hexagonal boron nitride induces anion trapping in a polyethylene oxide based solid polymer electrolyte for lithium dendrite inhibition. *J. Mater. Chem. A* **2020**, *8* (19), 9579−9589.
(16) Yin, X.; Wang, L.; Kim, Y.; Ding, N.; Kong, J.; Safanama, D.; Zheng, Y.; Xu, J.; Repaka, D. V. M.; Hippalgaonkar, K.; Lee, S. W.; Adams, S.; Zheng, G. W. Thermal conductive 2D Boron nitride for high-performance all-solid-state lithium−sulfur batteries. *Adv. Sci.* **2020**, *7* (19), 2001303.
(17) Liu, M.; Zhang, S.; Li, G.; Wang, C.; Li, B.; Li, M.; Wang, Y.; Ming, H.; Wen, Y.; Qiu, J.; Chen, J.; Zhao, P. A cross-linked gel polymer electrolyte employing cellulose acetate matrix and layered boron nitride filler prepared via in situ thermal polymerization. *J. Power Sources* **2021**, *484*, No. 229235.
(18) Doyle, M.; Fuller, T. F.; Newman, J. The importance of the lithium ion transference number in lithium/polymer cells. *Electrochim. Acta* **1994**, *39* (13), 2073−2081.
(19) Zhi, C.; Bando, Y.; Tang, C.; Kuwahara, H.; Golberg, D. Large-scale fabrication of boron nitride nanosheets and their utilization in polymeric composites with improved thermal and mechanical properties. *Advanced materials* **2009**, *21* (28), 2889−2893.
(20) Rasul, M. G.; Kiziltas, A.; Arfaei, B.; Shahbazian-Yassar, R. 2D boron nitride nanosheets for polymer composite materials. *npj 2D Materials and Applications* **2021**, *5* (1), 56.
(21) Terao, T.; Zhi, C.; Bando, Y.; Mitome, M.; Tang, C.; Golberg, D. Alignment of boron nitride nanotubes in polymeric composite films for thermal conductivity improvement. *J. Phys. Chem. C* **2010**, *114* (10), 4340−4344.
(22) Zhao, L.; Yan, L.; Wei, C.; Li, Q.; Huang, X.; Wang, Z.; Fu, M.; Ren, J. Synergistic enhanced thermal conductivity of epoxy composites with boron nitride nanosheets and microspheres. *J. Phys. Chem. C* **2020**, *124* (23), 12723−12733.
(23) Tong, Y.; Lin, Y.; Wang, S.; Song, M. A study of crystallisation of poly (ethylene oxide) and polypropylene on graphene surface. *Polymer* **2015**, *73*, 52−61.
(24) Sajid, M.; Kim, H. B.; Lim, J. H.; Choi, K. H. Liquid-assisted exfoliation of 2D hBN flakes and their dispersion in PEO to fabricate highly specific and stable linear humidity sensors. *Journal of Materials Chemistry C* **2018**, *6* (6), 1421−1432.
(25) Biccai, S.; Boland, C. S.; O'Driscoll, D. P.; Harvey, A.; Gabbett, C.; O'Suilleabhain, D. R.; Griffin, A. J.; Li, Z.; Young, R. J.; Coleman, J. N. Negative gauge factor piezoresistive composites based on polymers filled with $MoS_2$ nanosheets. *ACS Nano* **2019**, *13* (6), 6845−6855.
(26) Zhi, C.; Zhang, L.; Bando, Y.; Terao, T.; Tang, C.; Kuwahara, H.; Golberg, D. New crystalline phase induced by boron nitride nanotubes in polyaniline. *J. Phys. Chem. C* **2008**, *112* (45), 17592−17595.
(27) Fan, L.; Nan, C. W.; Zhao, S. Effect of modified $SiO_2$ on the properties of PEO-based polymer electrolytes. *Solid State Ionics* **2003**, *164* (1−2), 81−86.
(28) Zhang, H. H.; Maitra, P.; Wunder, S. L. Preparation and characterization of composite electrolytes based on PEO(375)-grafted fumed silica. *Solid State Ionics* **2008**, *178* (39−40), 1975−1983.
(29) Thakur, A. K.; Hashmi, S. A. Polymer matrix−filler interaction mechanism for modified ion transport and glass transition temperature in the polymer electrolyte composites. *Solid State Ionics* **2010**, *181* (27−28), 1270−1278.
(30) Chen, S.; Feng, F.; Yin, Y.; Lizo, X.; Ma, Z. Plastic crystal polymer electrolytes containing boron based anion acceptors for room temperature all-solid-state sodium-ion batteries. *Energy Storage Materials* **2019**, *22*, 57−65.
(31) Chen, S.; Feng, F.; Che, H.; Yin, Y.; Ma, Z. F. High performance solid-state sodium batteries enabled by boron contained 3D composite polymer electrolyte. *Chemical Engineering Journal* **2021**, *406*, No. 126736.
(32) Genier, F. S.; Pathreeker, S.; Adebo, P. O.; Chando, P.; Hosein, I. D. Design of a Boron-Containing PTHF-Based Solid Polymer Electrolyte for Sodium-Ion Conduction with High $Na^+$ Mobility and Salt Dissociation. *ACS Applied Polymer Materials* **2022**, *4* (10), 7645−7663.
(33) Yang, M.; Feng, F.; Ren, Y.; Chen, S.; Chen, F.; Chu, D.; Guo, J.; Shi, Z.; Cai, T.; Zhang, W.; Ma, Z.; Chen, S.; Liu, T. Coupling Anion-Capturer with Polymer Chains in Fireproof Gel Polymer Electrolyte Enables Dendrite-Free Sodium Metal Batteries. *Adv. Funct. Mater.* **2023**, 2305383.
(34) Ren, Y.; Yang, M.; Shi, Z.; Guo, J.; Chu, D.; Feng, F.; Li, H.; Ma, Z. F.; Chen, S.; Liu, T. A metalophilic, anion-trapped composite gel electrolyte enables highly stable electrode/electrolyte interfaces in sodium metal batteries. *Energy Storage Materials* **2023**, *61*, No. 102909.
(35) Sreekanth, T.; Jaipal Reddy, M.; Ramalingaiah, S.; Subba Rao, U. V. Ion-conducting polymer electrolyte based on poly (ethylene oxide) complexed with $NaNO_3$ salt-application as an electrochemical cell. *J. Power Sources* **1999**, *79* (1), 105−110.
(36) Anantha, P. S.; Hariharan, K. Physical and ionic transport studies on poly (ethylene oxide)−$NaNO_3$ polymer electrolyte system. *Solid State Ionics* **2005**, *176* (1−2), 155−162.


https://doi.org/10.1021/acs.jpcc.3c06455
J. Phys. Chem. C 2024, 128, 38−49

(37) Wu, Y.; Wagner, L. K.; Aluru, N. R. The interaction between hexagonal boron nitride and water from first principles. *J. Chem. Phys.* **2015**, *142* (23), 234702 DOI: 10.1063/1.4922491.
(38) Boys, S. F.; Bernardi, F. J. M. P. The calculation of small molecular interactions by the differences of separate total energies. Some procedures with reduced errors. *Mol. Phys.* **1970**, *19* (4), 553−566.
(39) Pipertzis, A.; Papamokos, G.; Sachnik, O.; Allard, S.; Scherf, U.; Floudas, G. Ionic conductivity in polyfluorene-based diblock copolymers comprising nanodomains of a polymerized ionic liquid and a solid polymer electrolyte doped with LiTFSI. *Macromolecules* **2021**, *54* (9), 4257−4268.
(40) Pipertzis, A.; Papamokos, G.; Mühlinghaus, M.; Mezger, M.; Scherf, U.; Floudas, G. What determines the glass temperature and dc-conductivity in imidazolium-polymerized ionic liquids with a polythiophene backbone? *Macromolecules* **2020**, *53* (9), 3535−3550.
(41) Gam, S.; Meth, J. S.; Zane, S. G.; Chi, C.; Wood, B. A.; Seitz, M. E.; Winey, K. I.; Clarke, N.; Composto, R. J. Macromolecular diffusion in a crowded polymer nanocomposite. *Macromolecules* **2011**, *44* (9), 3494−3501.
(42) Mutiso, R. M.; Winey, K. I. Electrical properties of polymer nanocomposites containing rod-like nanofillers. *Prog. Polym. Sci.* **2015**, *40*, 63−84.
(43) Kumar, S. K.; Benicewicz, B. C.; Vaia, R. A.; Winey, K. I. 50th anniversary perspective: Are polymer nanocomposites practical for applications? *Macromolecules* **2017**, *50* (3), 714−731.
(44) Celzard, A.; McRae, E.; Deleuze, C.; Dufort, M.; Furdin, G.; Marêché, J. F. Critical concentration in percolating systems containing a high-aspect-ratio filler. *Phys. Rev. B* **1996**, *53* (10), 6209.
(45) Wang, W.; Yi, E.; Fici, A. J.; Laine, R. M.; Kieffer, J. Lithium ion conducting poly (ethylene oxide)-based solid electrolytes containing active or passive ceramic nanoparticles. *J. Phys. Chem. C* **2017**, *121* (5), 2563−2573.
(46) Ban, X.; Zhang, W.; Chen, N.; Sun, C. A high-performance and durable poly (ethylene oxide)-based composite solid electrolyte for all solid-state lithium battery. *J. Phys. Chem. C* **2018**, *122* (18), 9852−9858.
(47) Ko, W. Y.; Lee, M. S.; Hsu, H. C.; Lin, K. J. One-Pot Green Synthesis of a PEO/TCPP/$LiClO_4$ Solid Polymer Electrolyte with Improvement of Ion Transport. *J. Phys. Chem. C* **2021**, *125* (42), 22960−22969.
(48) Chandrasekaran, R.; Selladurai, S. Preparation and characterization of a new polymer electrolyte (PEO:$NaClO_3$) for battery application. *J. Solid State Electrochem.* **2001**, *5*, 355−361.
(49) Chu, P. P.; Reddy, M. J.; Kao, H. M. Novel composite polymer electrolyte comprising mesoporous structured $SiO_2$ and PEO/Li. *Solid State Ionics* **2003**, *156* (1−2), 141−153.
(50) Pan, Q.; Zheng, Y.; Kota, S.; Huang, W.; Wang, S.; Qi, H.; Kim, S.; Tu, Y.; Barsoum, M. W.; Li, C. Y. 2D MXene-containing polymer electrolytes for all-solid-state lithium metal batteries. *Nanoscale Advances* **2019**, *1* (1), 395−402.
(51) Müller, A. J.; Arnal, M. L.; Trujillo, M.; Lorenzo, A. T. Supernucleation in nanocomposites and confinement effects on the crystallizable components within block copolymers, miktoarm star copolymers and nanocomposites. *Eur. Polym. J.* **2011**, *47* (4), 614−629.
(52) Huang, Z.; Wang, S.; Kota, S.; Pan, Q.; Barsoum, M. W.; Li, C. Y. Structure and crystallization behavior of poly (ethylene oxide)/$Ti_3C_2T_x$ MXene nanocomposites. *Polymer* **2016**, *102*, 119−126.
(53) Noor, S. A. M.; Ahmad, A.; Talib, I. A.; Rahman, M. Y. Morphology, chemical interaction, and conductivity of a PEO-ENR50 based on solid polymer electrolyte. *Ionics* **2010**, *16*, 161−170.
(54) Hiraoka, K.; Kato, M.; Kobayashi, T.; Seki, S. Polyether/$Na_3Zr_2Si_2PO_{12}$ composite solid electrolytes for all-solid-state sodium batteries. *J. Phys. Chem. C* **2020**, *124* (40), 21948−21956.
(55) Yang, L. Y.; Wei, D. X.; Xu, M.; Yao, Y. F.; Chen, Q. Transferring lithium ions in nanochannels: a PEO/$Li^+$ solid polymer electrolyte design. *Angew. Chem., Int. Ed.* **2014**, *53* (14), 3631−3635.
(56) Fu, X. B.; Yang, G.; Wu, J. Z.; Wang, J. C.; Chen, Q.; Yao, Y. F. Fast Lithium-Ion Transportation in Crystalline Polymer Electrolytes. *ChemPhysChem* **2018**, *19* (1), 45−50.
(57) Papke, B. L.; Ratner, M. A.; Shriver, D. F. Vibrational spectroscopy and structure of polymer electrolytes, poly (ethylene oxide) complexes of alkali metal salts. *J. Phys. Chem. Solids* **1981**, *42* (6), 493−500.
(58) Papke, B. L.; Dupon, R.; Ratner, M. A.; Shriver, D. F. Ion-pairing in polyether solid electrolytes and its influence on ion transport. *Solid State Ionics* **1981**, *5*, 685−688.
(59) Marcos, J. I.; Orlandi, E.; Zerbi, G. Poly (ethylene oxide)-poly (methyl methacrylate) interactions in polymer blends: an infra-red study. *Polymer* **1990**, *31* (10), 1899−1903.
(60) Yang, S.; Liu, Z.; Liu, Y.; Jiao, Y. Effect of molecular weight on conformational changes of PEO: an infrared spectroscopic analysis. *J. Mater. Sci.* **2015**, *50*, 1544−1552.
(61) Memboeuf, A.; Vékey, K.; Lendvay, G. Structure and energetics of poly (ethylene glycol) cationized by $Li^+$, $Na^+$, $K^+$ and $Cs^+$: a first-principles study. *European Journal of Mass Spectrometry* **2011**, *17* (1), 33−46.
(62) Hosseinian, A.; Khosroshahi, E. S.; Nejati, K.; Edjlali, E.; Vessally, E. A DFT study on graphene, SiC, BN, and AlN nanosheets as anodes in Na-ion batteries. *J. Mol. Model.* **2017**, *23*, 1−7.
(63) Mei, X.; Wu, Y.; Gao, Y.; Zhu, Y.; Bo, S. H.; Guo, Y. A quantitative correlation between macromolecular crystallinity and ionic conductivity in polymer-ceramic composite solid electrolytes. *Materials Today Communications* **2020**, *24*, No. 101004.
(64) Wieczorek, W.; Such, K.; Chung, S. H.; Stevens, J. R. Comparison of Properties of Composite Polymeric Electrolytes Based on the Oxymethylene-Linked Poly (ethylene oxide) $NaClO_4$ Electrolyte with Polyacrylamide or. alpha.-$Al_2O_3$ Additives. *J. Phys. Chem.* **1994**, *98* (36), 9047−9055.
(65) Karan, N. K.; Pradhan, D. K.; Thomas, R.; Natesan, B.; Katiyar, R. S. Solid polymer electrolytes based on polyethylene oxide and lithium trifluoro-methane sulfonate (PEO−$LiCF_3SO_3$): Ionic conductivity and dielectric relaxation. *Solid State Ionics* **2008**, *179* (19−20), 689−696.


https://doi.org/10.1021/acs.jpcc.3c06455
J. Phys. Chem. C 2024, 128, 38−49